Available online at www.sciencedirect.com
SCIENCE DIRECT
International Journal of Heat and Fluid Flow 27 (2006) 737–746
International Journal of HEAT AND FLUID FLOW
www.elsevier.com/locate/ijhff

Simultaneous measurements of fluctuating velocity and pressure in a turbulent mixing layer

Yoshitsugu Naka [a], Takeshi Omori [b], Shinnosuke Obi [a,*], Shigeaki Masuda [a]

[a] Department of Mechanical Engineering, Keio University, Hiyoshi 3-14-1, Kohoku-ku, Yokohama 223-8522, Japan
[b] Chair of Fluid Mechanics and Aerodynamics, Darmstadt University of Technology, Petersenstr. 30, 64287 Darmstadt, Germany

Available online 18 April 2006

Abstract

A novel experimental technique to measure static pressure fluctuation was applied in order to evaluate velocity–pressure correlation in a turbulent mixing layer. The developing region of the mixing layer was found to be out of equilibrium state, indicating the oscillatory velocity fluctuation due to vortex shedding and remarkable production of turbulence. The contribution of pressure-related terms in the transport equation of the Reynolds stress is found to be well captured by the present method. A simple model for pressure diffusion by Lumley gave a satisfactory approximation when the flow approached the self-similar state. However, the analogy between pressure diffusion and turbulent diffusion becomes weaker when the flow exhibits characteristics which are not found in the equilibrium state.

Keywords: Measurement method; Non-equilibrium free shear layer; Velocity–pressure correlation

1. Introduction

The importance of pressure fluctuation in turbulent flows has long been recognized and is still one of the unanswered questions in turbulence research. A number of experiments show that the correlation between fluctuating pressure and velocity, originating from large-scale vortex structures, plays a significant role in determining the budget of transport equations for turbulence properties. Numerous computational approaches have made great contributions towards the understanding of the dynamics of the inviscid flow and organized motion of vortices, but it is too complex to give the whole description of turbulent motions. Although there are lot of suggestions on the close relationships between pressure fluctuation and coherent turbulent fluid motion, the interaction of the velocity and pressure should be explored from various viewpoints.

Problems in the currently available turbulence models lie in the lack of physical characterization of the velocity–pressure correlation, particularly when the turbulence structure departs from the equilibrium state of turbulent kinetic energy. The conditions of flow out of the equilibrium state is far from ideal; one where calibrations of turbulence models are often undertaken, e.g., isotropic, homogeneous, or simple shear flows. As a consequence, the performance of existing models in predicting complex flows is not well established, unlike the case of simple shear flows. In order to develop better turbulence models for prediction of non-equilibrium flows, the key mechanism which is governed by the pressure-related turbulent motions must be addressed.

There are numerous efforts available for both experimental and computational approaches to understand the role of pressure fluctuation. Relatively little experimental researches about pressure-related statistics is available, mainly because of underlying technical difficulties in measuring static pressure fluctuation at arbitrary locations in the flow field. In his pioneering work, Kobashi (1957) combined the condenser microphone with a static pressure tube, and represents a step towards the evaluation of fluctuating pressure. With reference to his work, Shirahama and Toyoda (1993) developed a probe to measure fluctuating

* Corresponding author. Tel.: +81 45 566 1499; fax: +81 45 566 1495.
E-mail address: obsn@mech.keio.ac.jp (S. Obi).

0142-727X/$ - see front matter © 2006 Elsevier Inc. All rights reserved.
doi:10.1016/j.ijheatfluidflow.2006.02.023

Nomenclature

C	electronic capacitance of condenser microphone
D_{ij}^{t}, D_{ij}^{p}, D_{ij}^{v}	turbulent, pressure and viscous diffusion of Reynolds stress
f	frequency of fluctuating pressure
G_v	power spectrum density of normal velocity component v
p^*	non-dimensional fluctuating pressure, $= p/(\rho U_s^2)$
P_{ij}	production rate of Reynolds stress
$\overline{p^2}$	second-moment of pressure fluctuation
R	input resistance of main amplifier for microphone
$R_{u_iu_j}$, R_{u_ip}	correlation coefficient
Re	Reynolds number of oncoming turbulent boundary layers, based on free stream velocity and momentum thickness
St	Strouhal number based on thickness of splitter plate edge and U_s
S	expansion factor of mixing layer, $=(U_c/U_s)(\Delta\delta/\Delta x)$
Tu_f	free-stream turbulence intensity
U, V	streamwise and transverse mean velocity components
U_c	convective velocity, $=(U_h + U_l)/2$
U_s	difference of free stream mean velocity, $= U_h - U_l$
u, v	fluctuating velocity components in the x and y directions
$\hat{u}$	instantaneous streamwise velocity component
u^*, v^*	non-dimensional velocity components, $u^* = u/U_s$ and $v^* = v/U_s$
$\overline{u'^2}$	non-dimensional streamwise velocity fluctuation, $= \overline{u^2}/\overline{u_\infty^2}$
$\overline{u_iu_j}$	Reynolds stress
$\overline{u_ip}$	velocity–pressure correlation
$\overline{u_iu_ju_k}$	triple velocity correlation
x, y, z	Cartesian coordinates in streamwise, transverse and spanwise directions

Greeks

δ	thickness of mixing layer
δ_b	99% thickness of oncoming boundary layer
Δx	streamwise distance between measurement locations
Δz	spanwise distance between velocity and pressure probes
$\Delta\delta$	rate-of-development of mixing layer thickness
ε_{ij}	dissipation rate of Reynolds stress
η_θ	non-dimensional transverse coordinate, $= y/\theta$
θ	momentum thickness of mixing layer at $x = 100$ mm
θ_d	phase correction of pressure signal
ρ	fluid density
Φ_{ij}	re-distribution of Reynolds stress

Subscripts

$()_h$	quantities in high speed side
$()_l$	quantities in low speed side

pressure with sufficient accuracy in free shear flows. This type of pressure probe enabled an evaluation of fluctuating pressure, for example, Tsuji and Ishihama (2003) introduced this probe to reveal the power-law and proportional constant of normalized pressure spectrum. A recent study by Tsuji et al. (2005) reports a successful application of the technique in measuring the turbulent boundary layer.

The progress in computer technology has enabled direct numerical simulations (DNS) to be applied to increasingly complex flows with spatial development which contains remarkably large pressure fluctuation in contrast to simple flows. Yao et al. (2001) indicated in their DNS study on the transition from turbulent boundary layer along a flat plate to free shear layer that there are remarkable differences in the common features found in the fully developed channel flow. A temporally developing turbulent mixing layer was calculated by Rogers and Moser (1994) and it was indicated that both of the large scale rollers and finer scale ribs play an important role in representing the properties of the shear layer. Nevertheless, both computational and experimental approaches are required to better understand the role of pressure fluctuation in turbulent shear flows.

The present study focuses on the experimental approach to a relatively simple turbulent shear flow but out of an equilibrium state of turbulence. A spatially developing turbulent mixing layer is selected as the test case, where the gradual development of the oncoming turbulent boundary layer flow to the free shear flow is investigated. Particular attention is paid to the transitional stage of the kinetic energy balance through the non-equilibrium region before the shear layer develops to a self-similar state, as schematically shown in Fig. 1. An advanced technique for the simultaneous measurement of velocity and pressure is presented, which is based on our previous work (Omori et al., 2003), and discussions are presented on the existing simple model of pressure-diffusion transport of Reynolds stresses.

Special attention is paid to retain the accuracy in the measurement of velocity–pressure correlation which is severely affected by temporal and spatial lags between two different signals. A phase-correction formula for the pressure signal, which is constructed by the information provided by the manufacturer, is introduced in the present study. Additionally, the inevitable effects of spatial interference between sensors is systematically investigated and

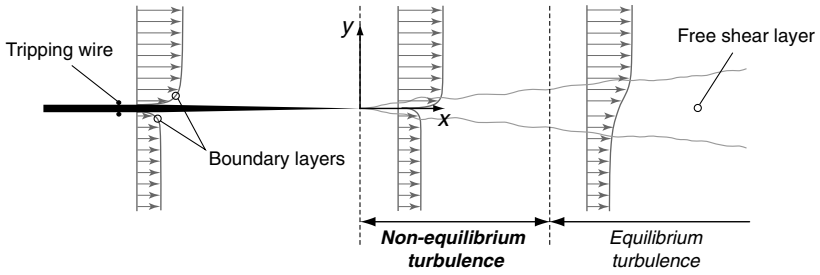

Fig. 1. Schematics of the considered flow field.

explained in the following section, preceding the detailed discussion on the pressure-related turbulence statistics.

2. Experiments

2.1. Setup and instruments

The wind tunnel that was specially designed for the turbulent mixing layer experiments was used (Omori et al., 2003). The inlet section of the tunnel was divided into two parallel parts, and the fully developed turbulent boundary layers merged at the test section of the 0.5 m × 0.5 m cross section. The orthogonal coordinate system, originating from the trailing edge of the splitter plate, was defined, with the x- and y-axes taken in streamwise and transverse directions, respectively, see Fig. 1. The mixing layer was found to be uniform for at least 70% of the span, corresponding to 10 times of the mixing layer thickness.

The conditions of the oncoming inlet boundary layers, measured at $x = -50$ mm, is summarized in Table 1. Tu_f is the turbulence intensity outside the boundary layer and δ_b stands for the 99% thickness of the boundary layer. The Reynolds number Re is based on the free stream velocity U and the momentum thickness.

According to Shirahama and Toyoda (1993), a thin static pressure probe was used for the fluctuating pressure measurements, see Fig. 2. The probe was set parallel to the flow direction so the static pressure fluctuation sensed at the four small holes on the side of the 1.0 mm thick pipe was measured. The pressure fluctuation was converted to an electric signal by a condenser microphone (RION UC-29) which was mounted on the end of the probe. The performance of the present method was investigated in detail in our preceding work (Omori et al., 2003).

Table 1
Inlet conditions

	U [m/s]	Tu_f [%]	δ_b [mm]	Re
High speed side	7.2	0.76	18.8	610
Low speed side	3.3	0.94	18.8	260

The fluctuating velocity was measured by a hot-wire anemometer (HWA). A commercial X-wires probe (Dantec 55P64) was used for two-component velocity measurements, combined with a constant temperature anemometer (CTA, Kanomax 1011). The microphone and the HWA-probe were mounted on a common unit to facilitate the traversing of them to arbitrary positions. The distance between static pressure tube and X-wires probe was adjusted by using a digital micro-scope (Keyence VH-6200) prior to every run. The signal from the CTA and the main amplifier of the microphone were transferred to a PC through a 16bit-A/D converter (National Instruments PCI-MIO-16XE-10). All data acquisition was managed by LabView™ (National Instruments) and further data processing was handled by programs written in Matlab™.

A look-up table method by Lueptow et al. (1988) was adopted to convert the signal of X-wires HWA to velocity data. The calibration of the HWA signal was performed by a resolution of 0.3 m/s, ranging from 2.5 m/s to 6.8 m/s; the resolution in direction was 3°, covering from −30° to 30° with respect to the main flow direction. Third-order polynomials were used to fit the curves on the plane composed of a pair of X-wires sensor voltage to obtain velocity variations for arbitrary angle of attack. The resulting look-up table had 80 intervals covering the full range in each

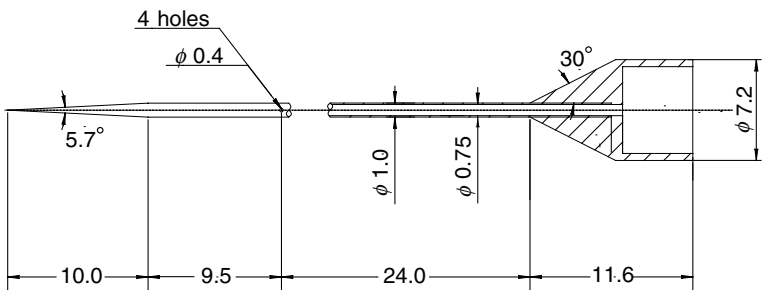

Fig. 2. Schematic of the static pressure tube (dimensions in mm).

sensor voltage, where the desired pair of velocity and angle was sought by use of a bi-linear interpolation function available in the Matlab™ library.

2.2. Noise reduction and phase correction practice

In order to reduce the influence of background noise in the wind tunnel, the pressure signal outside the mixing layer was monitored simultaneously by an auxiliary pressure probe which had the identical dimensions as that used for the measurements in the shear layer. The signal acquired by the secondary probe was subtracted from that obtained in the shear layer so that only the desired local pressure related to turbulent fluid motion could be extracted. The effect of such a practice is demonstrated in Fig. 3. The plots after the procedure (marked as "differential") show a remarkable reduction of background noise in fluctuating pressure $\overline{p^2}$ in the free stream as compared to the raw data.

Another factor, which contaminates the estimation of the velocity–pressure correlation, lies in the phase-lag between velocity and pressure signal. The phase-lag that depends on the frequency is caused by the electric circuit of the condenser microphone system. In the present study, an analytical formula is introduced to correct this phase-lag:

$$\theta_d = \pi - \tan^{-1}\left(\frac{1}{2\pi CRf}\right), \tag{1}$$

where C is electronic capacitance of the condenser microphone, R stands for the input resistance of main amplifier of the microphone, and f denotes the frequency of the fluctuating pressure. In the present study, C and R are 6 pF and 3 GΩ, respectively, according to the hardware specifications.

The effect of the correction is demonstrated in Fig. 4; the compensated velocity–pressure correlation shows a profile which takes a sign opposite to that of the value without correction. It is rather surprising that the effect of the correction is not a slight fraction but remarkable in a qualitative manner. The results shown hereafter are only those after these correction practices, i.e., differential noise reduction and phase-lag correction.

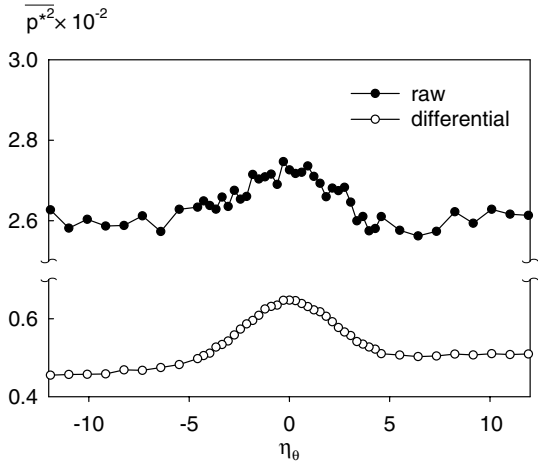

Fig. 3. Effect of noise reduction on the fluctuating pressure measured at $x = 100$ mm.

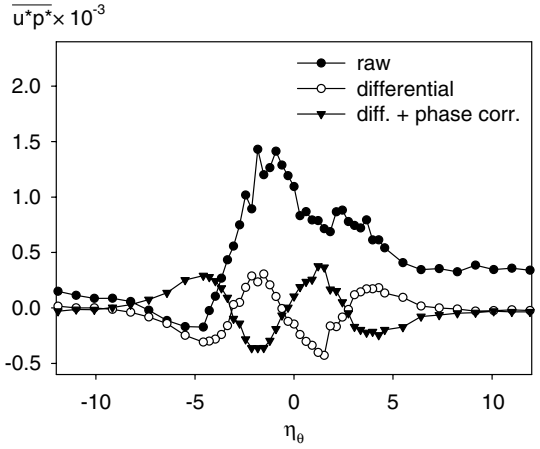

Fig. 4. Corrected velocity–pressure correlations ($x = 100$ mm).

2.3. Interference of probes

The inevitable effects due to the departure of the pressure probe and the X-wires sensor on the measured velocity–pressure correlation have been investigated. In order to achieve a precise correlation, the two sensors used to measure each quantity should be set as close as possible to each other. On the other hand, using too close of a distance causes interference between the probes and eventually contaminates the signal. To determine the minimum distance between the probes where the sensors are free from the interference, we have measured the velocity fluctuation as a function of the probe distance Δz, where the z-coordinate is directed in the spanwise direction.

Fig. 5 shows the streamwise velocity fluctuation measured by the X-wires probe, comparing those taken when the pressure probe is set aside (the plots "P–X") with those when the pressure probe is replaced by an I-type HWA sen-

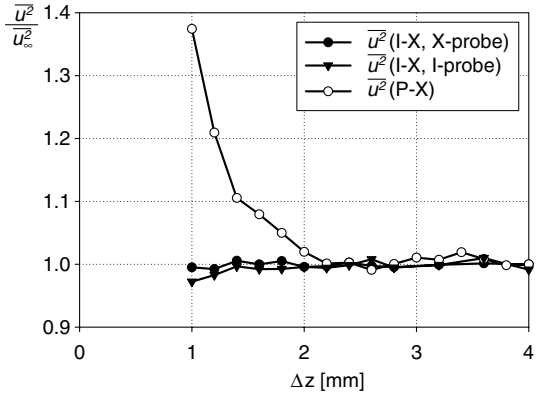

Fig. 5. The interference of probe distance ($x = 100$ mm).

sor (“I–X, X-probe”), and, for reference, also with the data taken by the same I-type HWA in the proximity of the X-wires HWA (“I–X, I-probe”); the last plots may represent the disturbance due to the X-wires probe on the location of the pressure measurement. The measurements are undertaken at $x = 100$ mm and $y = 2.1$ mm where the velocity–pressure correlation $\overline{u^* p^*}$ is found to reach the maximum, as explained later. It is clear that the existence of the pressure probe strongly influences the velocity measurement by the X-wire sensor, as indicated by the steep increase of $\overline{u'^2}$ (P–X) for $\Delta z \leqslant 2$ mm. On the other hand, the data taken by the X- and I-type sensors in absence of the pressure probe show constant values down to $\Delta z \sim 1$ mm. It is inferred that the hot-wire sensors are small enough to prevent interference on the pressure measurements. Based on these arguments, the probe distance is fixed to 2 mm in the present study.

It is reasonable to consider that the measured velocity–pressure correlations are somewhat lower than the true values because of the finite distance between the probes. A rough estimation of this possible under-estimation is performed by referencing the two-point velocity correlation measured by the previously mentioned HWA-sensor combinations at the same location, see Fig. 6. The two-point correlation of the streamwise velocity fluctuation, R_{uu}, indicates a monotonic increase with the decreasing Δz. It should reach unity for the limit of $\Delta z = 0$, and the plots show a reasonable asymptotic tendency to this value. It should be noted that the distance between the sensors of X-wires itself is 1 mm, hence the data for Δz below 1 mm is not meaningful and not shown. The value of R_{uu} is about 0.6 at $\Delta z = 2$ mm, which implies that the velocity–pressure correlation measured for the probe distance of 2 mm may under-estimate the true value by 40%. On the other hand, the limiting value of the correlation between streamwise- and transverse-components of the fluctuating velocity, $-R_{uv}$, is approximately 0.45 at $\Delta z = 0$ in simple free shear layers (Bell and Mehta, 1990), and $-R_{uv}$ at $\Delta z = 2$ mm is smaller than this value by about 15%. From these observations, it is reasonable to conclude that the under-estimation

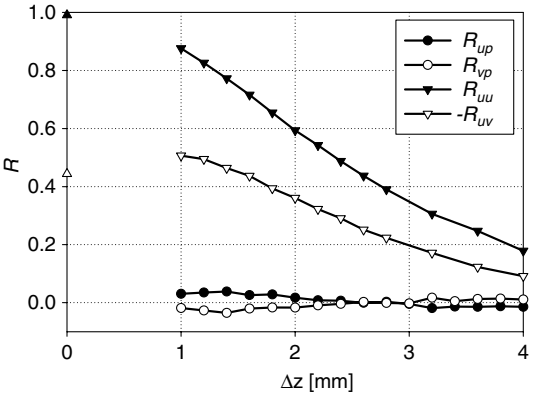

Fig. 6. Correlation coefficient of velocity–velocity and velocity–pressure ($x = 100$ mm).

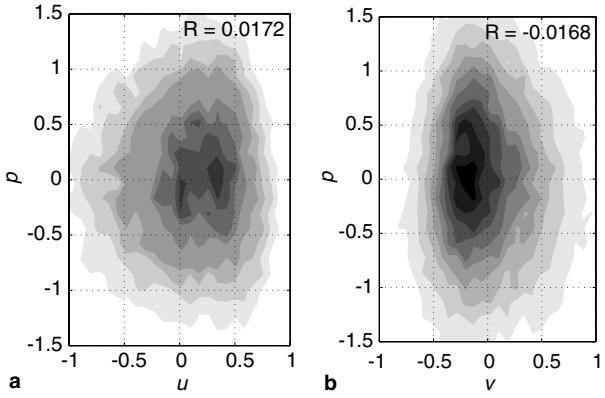

Fig. 7. Joint-pdf of (a) u and p; (b) v and p ($x = 100$ mm).

of the velocity–pressure correlation measured in the present study may be on the order of 30%.

The plots for the variation of the velocity–pressure correlations, R_{up} and R_{vp}, drawn in the same figure indicate a slight increase of these quantities for Δz smaller than 2 mm, though these are a consequence of the increase in velocity fluctuation and do not necessarily indicate an increase in the correlation, i.e., the convergence to the true values. A closer investigation into the correlation map (joint probability density function) of the fluctuating velocity and pressure shown in Fig. 7 indicates that these quantities are not correlated as well as one might expect. A small fraction of the correlation coefficients, which are on the order of 10^{-2} as indicated in the figure, are due to the slight off set of the peak of the joint probability density function. It is easily understood that the small disturbance in velocity fluctuation alone results in an apparent increase in the correlation. The velocity–pressure correlation is a delicate quantity even in the highly turbulent flow regime.

2.4. Data processing

The statistics were calculated from 80,000 samples. A sampling rate of 4 kHz was selected to evaluate quantities that require high temporal resolution, such as energy spectra and derivatives with respect to time. For other statistics the sampling rate was fixed to 200 Hz which was found to be sufficiently high from the examination of auto-correlation of the velocity fluctuation. The resulting integration time was 400 s for turbulence statistics. Typically, it took about an hour by PC (Pentium4 2.8 GHz) to complete the post-processing of each measurement to draw a profile, comprising 48 points, across the mixing layer.

3. Results

3.1. Primary remarks

The velocity profiles across the shear layer are measured at three different streamwise locations, $x = 25$ mm, 50 mm and 100 mm. The development of the shear layer thickness,

δ, was examined by means of the expansion factor of the free shear layer, $S = (U_c/U_s)(\Delta\delta/\Delta x)$ (Pope, 2000), with U_c being the convective velocity defined by $U_c = (U_h + U_l)/2$ where U_h and U_l are the free stream velocity of higher and lower velocity side, respectively, and U_s is the velocity difference, $U_s = U_h - U_l$. The value of S slightly decreases from 0.089, which is evaluated at the interval between 25 mm $\leqslant x \leqslant$ 50 mm, down to 0.086 at 50 mm $\leqslant x \leqslant$ 100 mm. The variation of S indicates that the shear layer is still under the development state.

3.2. Statistics of non-equilibrium turbulent mixing layer

The streamwise mean velocity profiles are shown in Fig. 8. The velocity U^* is normalized by the velocity difference U_s ($U^* = (U - U_l)/U_s$), and the non-dimensional coordinate η_θ is calculated using the momentum thickness of the shear layer at $x = 100$ mm ($\eta_\theta = y/\theta$). It should also be noted that η_θ is geometrically fixed to the center of the splitter plate. The wake of the splitter plate is observed at all locations, in contrast to the profile of DNS by Rogers and Moser (1994) representing the self-similar state. The deficit in the velocity profile reaches $0.18U_s$ at $x =$ 25 mm; it decreases down to $0.07U_s$ at 50 mm and still persists in the most downstream location, providing a slight under-shoot of the lower velocity side by $0.02U_s$ at $x = 100$ mm.

Fig. 9 presents the profiles of the individual Reynolds stress component at the same location as for Fig. 8. It is shown that every component decreases downstream, with the $\overline{v^2}$-component indicating a slightly faster decrease when compared to the others. The values are still considerably higher than the reference DNS values even at the most downstream location. As the shear layer spreads in the direction of lower velocity side, or towards negative η_θ, the distribution becomes broader and asymptotes to symmetrical shape for all of the components. It is worth noting that the shear stress $\overline{uv}$ changes sign in the narrow region in accordance with the mean velocity distribution that exhibits a distinct wake-like shape.

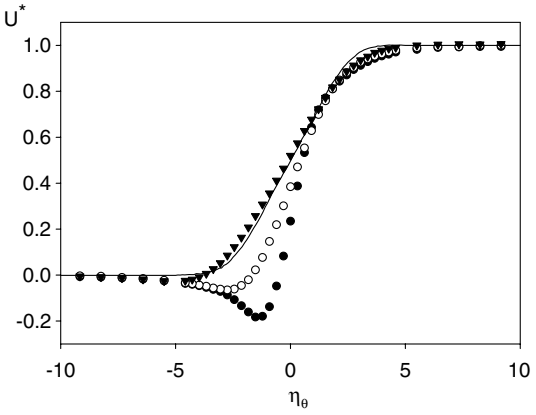

Fig. 8. Profile of the streamwise mean velocity; Symbols (●) $x = 25$ mm, (○) $x = 50$ mm, (▼) $x = 100$ mm, (—) DNS result of Rogers and Moser (1994).

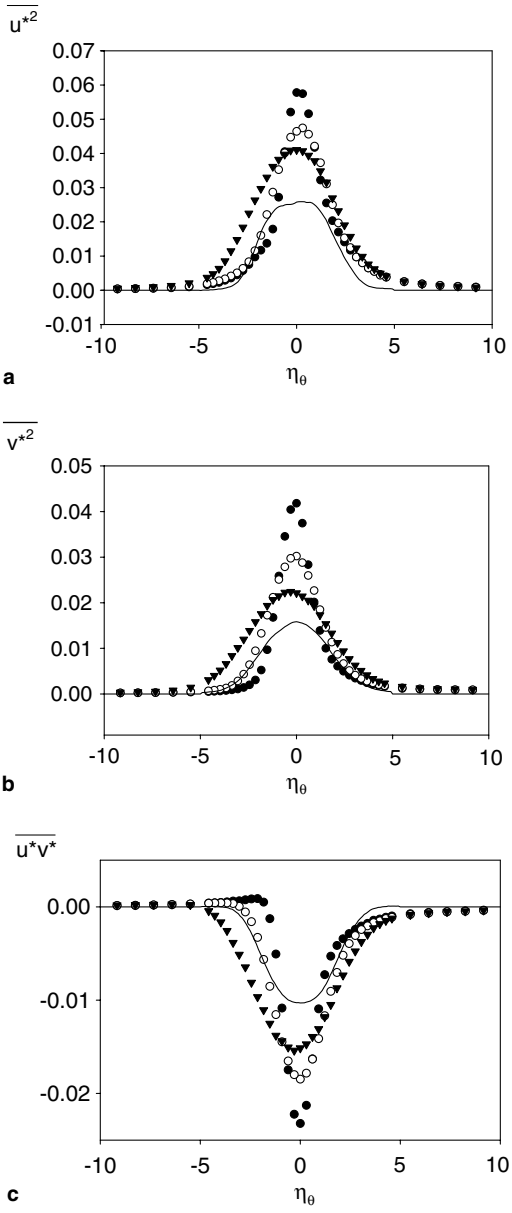

Fig. 9. Components of Reynolds stress tensor; (a) $\overline{u^2}$, (b) $\overline{v^2}$, (c) $\overline{uv}$; Symbols (●) $x = 25$ mm, (○) $x = 50$ mm, (▼) $x = 100$ mm, (—) DNS result of Rogers and Moser (1994).

The flow characteristics are further explored by means of the power spectrum density of the normal velocity component v, see Fig. 10, evaluated at $\eta_\theta = 0$. At the most upstream location, the distribution shows a peak near 330 Hz which corresponds to $St = 0.083$, with St being the Strouhal number based on the thickness of the splitter plate and U_s. Weaker peaks are also observed near 260 Hz and 160 Hz at $x = 50$ mm and 100 mm, respectively.

The characteristic frequency shown by the spectra is an indication of vortex shedding at a constant frequency, and the observed gradual decrease of the characteristic

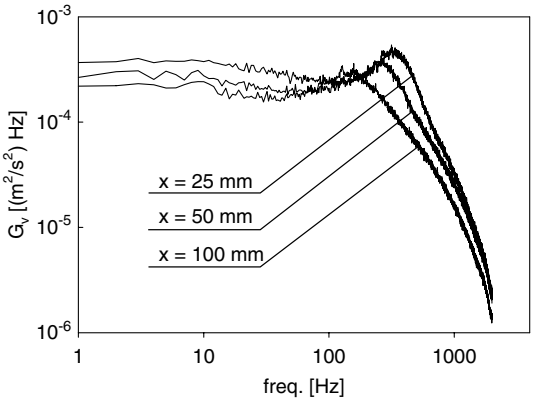

Fig. 10. Power spectrum density of v.

frequency is likely a consequence of vortex merging which occurs in the development stage. The DNS by Yao et al. (2001) reports a remarkable vortex shedding in the wake of a blunt body, with the Strouhal number 0.118 evaluated right behind the plate. Fig. 11 indicates streamwise variation of the characteristic frequency, and it is reasonable to consider that the periodic vortex shedding also exists in the present study especially near the trailing edge of the splitter plate. The influence of the vortex shedding gradually decays as the flow approaches to the self-similar state.

3.3. Velocity–pressure correlation in the shear layer

Fig. 12 shows the velocity–pressure correlations $\overline{up}$ and $\overline{vp}$, which are directly measured by the present method, compared to those evaluated by Lumley's model (1978) based on the triple-velocity correlation at the previously mentioned three streamwise locations:

$$\overline{up} = -\frac{1}{5}\left(\overline{u^3} + \overline{uv^2}\right), \tag{2}$$

$$\overline{vp} = -\frac{1}{5}\left(\overline{u^2 v} + \overline{v^3}\right). \tag{3}$$

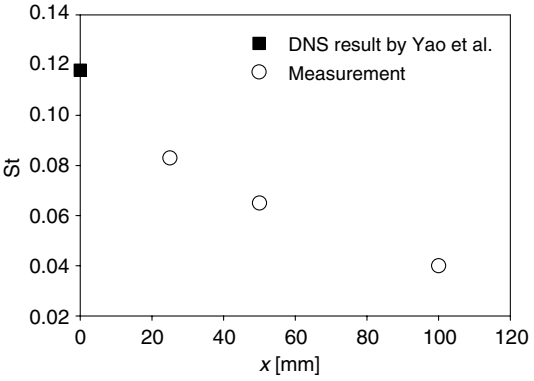

Fig. 11. Variation of Strouhal number.

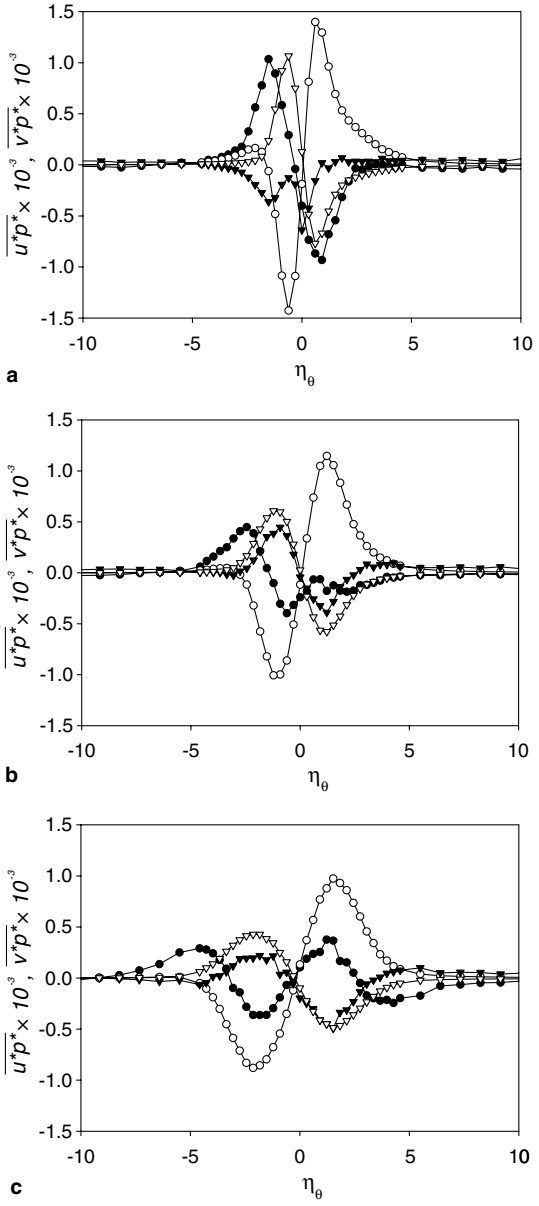

Fig. 12. Profiles of $\overline{up}$ and $\overline{vp}$; (a) $x = 25$ mm, (b) $x = 50$ mm, (c) $x = 100$ mm; Symbols (●) $\overline{up}$, (○) $\overline{up}$ (Lumley model), (▼) $\overline{vp}$, (▽) $\overline{vp}$ (Lumley model).

It is shown that both $\overline{up}$ and $\overline{vp}$ significantly vary across the shear layer, changing their sign at the center, and $\overline{up}$ consistently exceeds $\overline{vp}$ in magnitude. The gradual decay of all quantities is also observed in downstream when comparing (a), (b) and (c).

Lumley's model provides relatively fair agreement for both components at the locations shown in Fig. 12(b) and (c). An obvious departure is, however, evident in Fig. 12(a) that is measured at the most upstream location, where Lumley's model yields an opposite sign for $\overline{up}$, and the magnitude of $\overline{vp}$ is over-estimated. These disagreements may be related to the existence of the characteristic frequency in the power density of the velocity fluctuation v, see Fig. 10.

4. Discussion

The significance of the velocity–pressure correlation is further investigated in terms of the transport equation of the Reynolds stress:

$$\rho\frac{\mathrm{D}\overline{u_iu_j}}{\mathrm{D}t} = P_{ij} + (D^{\mathrm{t}}_{ij} + D^{\mathrm{p}}_{ij} + D^{\mathrm{v}}_{ij}) + \Phi_{ij} - \varepsilon_{ij}, \tag{4}$$

where the terms on the right hand side, P_{ij}, D_{ij}, Φ_{ij}, and ε_{ij} represent production, diffusion, re-distribution and dissipation of the Reynolds stress $\overline{u_iu_j}$. Among the three diffusion transports, the molecular viscous transport D^{v}_{ij} may be neglected because of a large Reynolds number; the other two, i.e., the turbulent diffusion D^{t}_{ij} and the pressure diffusion D^{p}_{ij}, are of equal importance and primary concern. Table 2 summarizes some representative terms in the equation which are evaluated in the present study. Because of the restriction of the available quantities, only the terms on the right column of the table are evaluated. Also note that Taylor's hypothesis is applied to the estimation of the re-distribution term in the equation for the $\overline{u^2}$-component,

$$\Phi_{11} = 2p\overline{\frac{\partial u}{\partial x}} \simeq -2p\overline{\frac{\mathrm{d}u}{\mathrm{d}t}\frac{1}{\hat{u}}}, \tag{5}$$

with $\hat{u}$ being the instantaneous streamwise velocity component.

Fig. 13 presents the distribution of production and the re-distribution term in the $\overline{u^2}$-equation at three streamwise locations. The DNS result of Rogers and Moser (1994) are shown for reference to the equilibrium state. It is seen that the production rate far exceeds the re-distribution at $x = 25$ mm, though rapidly decreases in the downstream. At the most downstream location, $x = 100$ mm in (c), the measured values coincide well with the DNS result. It is found that the evaluated re-distribution term is consistently smaller than the production in magnitude. It should be noted that there is a narrow region, $-3 \leqslant \eta_\theta \leqslant -1$ at $x = 25$ mm (a), where the production and re-distribution show opposite signs.

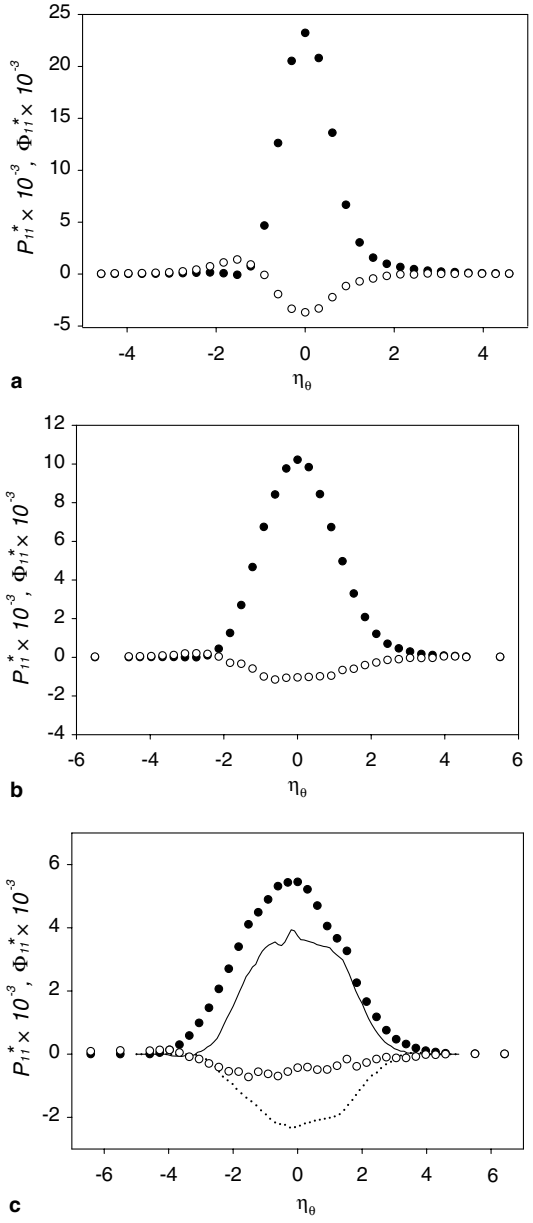

Fig. 13. Estimated re-distribution Φ_{11}; (a) $x = 25$ mm, (b) $x = 50$ mm, (c) $x = 100$ mm; Symbols (●) P_{11}, (○) Φ_{11}, (—) P_{11} (DNS), (···) Φ_{11} (DNS), DNS data of Rogers and Moser (1994).

Table 2
Terms of Reynolds stress equation

	Exact form	Present form
P_{11}	$-2\rho(\overline{u^2}\frac{\partial U}{\partial x} + \overline{uv}\frac{\partial U}{\partial y})$	$-2\rho\overline{uv}\frac{\partial U}{\partial y}$
Φ_{11}	$2p\overline{\frac{\partial u}{\partial x}}$	$-2p\overline{\frac{\mathrm{d}u}{\mathrm{d}t}\frac{1}{\hat{u}}}$
P_{12}	$-\rho\left(\overline{u^2}\frac{\partial V}{\partial x} + \overline{v^2}\frac{\partial U}{\partial y}\right)$	$-\rho\overline{v^2}\frac{\partial U}{\partial y}$
D^{t}_{12}	$-\rho\left(\frac{\partial\overline{u^2v}}{\partial x} + \frac{\partial\overline{uv^2}}{\partial y}\right)$	$-\rho\frac{\partial\overline{uv^2}}{\partial y}$
D^{p}_{12}	$-\left(\frac{\partial\overline{pv}}{\partial x} + \frac{\partial\overline{pu}}{\partial y}\right)$	$-\frac{\partial\overline{pu}}{\partial y}$
P_{22}	$-2\rho\left(\overline{vu}\frac{\partial V}{\partial x} + \overline{v^2}\frac{\partial V}{\partial y}\right)$	$-2\rho\overline{v^2}\frac{\partial V}{\partial y}$
D^{t}_{22}	$-\rho\left(\frac{\partial\overline{u^2}}{\partial x} + \frac{\partial\overline{u^2v}}{\partial y}\right)$	$-\rho\frac{\partial\overline{u^2v}}{\partial y}$
D^{p}_{22}	$-2\frac{\partial\overline{pv}}{\partial y}$	$-2\frac{\partial\overline{pv}}{\partial y}$

The balance of the representative terms are also presented for the $\overline{uv}$- and $\overline{v^2}$-components in Figs. 14 and 15, respectively. For both components, the production P_{ij}, turbulent diffusion D^{t}_{ij} and pressure diffusion D^{p}_{ij} are compared. Similarly to the case for the $\overline{u^2}$-component, the production term is over-proportional to the others at the most upstream location, $x = 25$ mm, and rapidly decreases in the downstream. In particular, the production of $\overline{v^2}$, Fig. 15(a), exhibits remarkable magnitude, which is not the case for the self-similar state where the production P_{22} nearly vanishes.

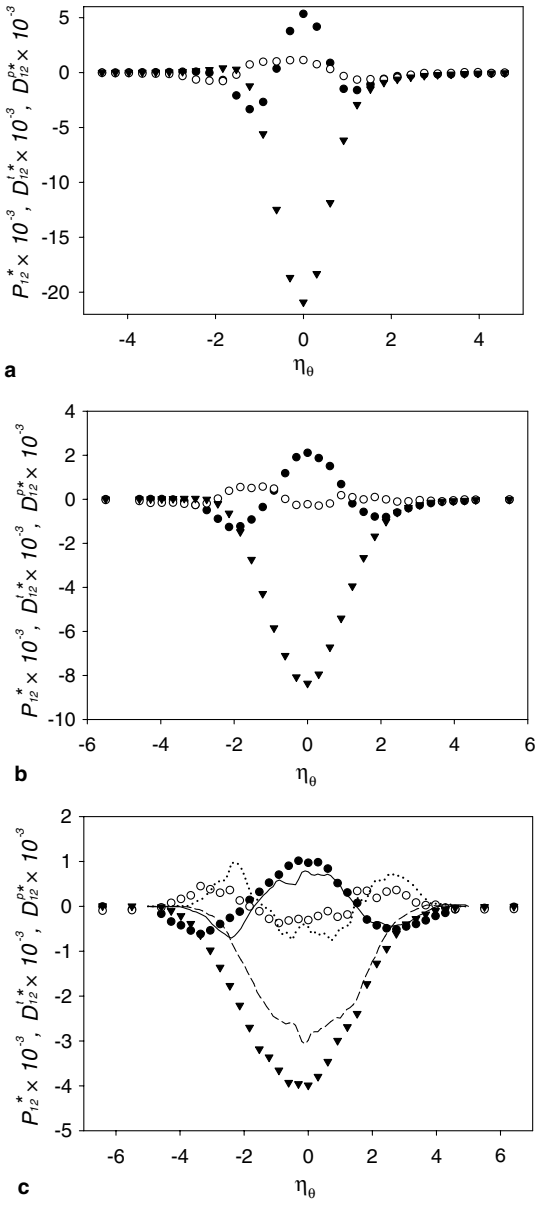

Fig. 14. Estimated turbulent-diffusion D_{12}^{t} and pressure-diffusion D_{12}^{p}; (a) $x = 25$ mm, (b) $x = 50$ mm, (c) $x = 100$ mm; Symbols (●) D_{12}^{t}, (○) D_{12}^{p}, (▼) P_{12}, (—) D_{12}^{t} (DNS), (···) D_{12}^{p} (DNS), (---) P_{12} (DNS).

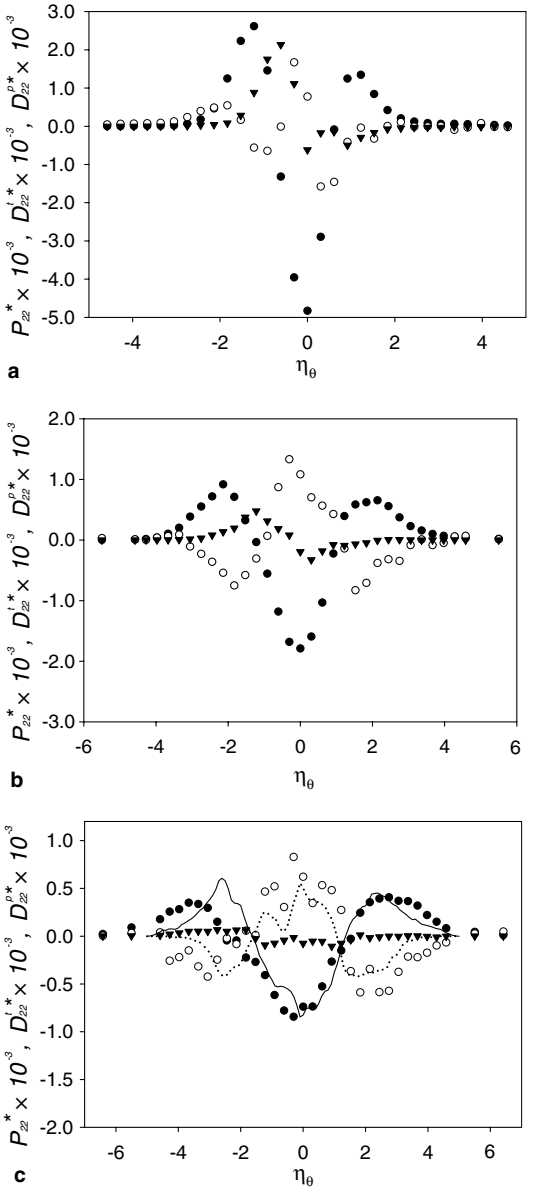

Fig. 15. Estimated turbulent-diffusion D_{22}^{t} and pressure-diffusion D_{22}^{p}; (a) $x = 25$ mm, (b) $x = 50$ mm, (c) $x = 100$ mm; Symbols (●) D_{22}^{t}, (○) D_{22}^{p}, (▼) P_{22}, (—) D_{22}^{t} (DNS), (···) D_{22}^{p} (DNS).

The two diffusion terms, turbulent- and pressure-diffusion, of these two components indicate reasonable proportion; they are opposite in sign and the turbulent diffusion is consistently larger than its counterpart across the shear layer. Again, the situation at the most upstream location, $x = 25$ mm in Fig. 15, is a little different from the other two downstream locations, where the analogy between the turbulent- and pressure-diffusion is not likely to hold.

The above discussion points to the fact that the relatively simple approximation of the pressure diffusion by Lumley (1978) well represents the simple shear flow close to the self-similar state. However, the analogy between the turbulent- and pressure-diffusion gradually breaks down as the flow starts to exhibit certain characteristics such as the existence of vortex shedding, or the departure from the equilibrium state. The role of pressure fluctuation becomes more important as the complexity of turbulence structure increases.

5. Concluding remarks

The experimental evaluation of the pressure-related turbulence statistics has been undertaken in a free mixing layer out of equilibrium state. The noise reduction as well as phase-lag correction procedures are shown to be successful in evaluating the fluctuating pressure and the correlation between velocity and pressure. The distance between the pressure probe and X-wires has been carefully adjusted

to minimize the interference and at the same time to retain the spatial resolution.

The characteristics of a spatial developing turbulent mixing layer were investigated with particular focus on the pressure-related quantities. Fundamental statistics are presented, and it is indicated that the flow characteristics are under development, showing remarkable velocity oscillation inherent to vortex shedding from the splitter plate. Velocity–pressure correlations are directly measured and compared with Lumley's model. The value of the Reynolds stress transport equation is examined, and the measured pressure-related terms were found to be in fair agreement with available DNS data. The analogy between the turbulent diffusion and pressure diffusion does not seem to hold in the region where the turbulence structure departs from that in the energy equilibrium state.

Acknowledgements

The authors are grateful to Prof. K. Toyoda of Hokkaido Institute of Technology, Japan, for invaluable discussions. A part of the present study was financially supported by the Ministry of Education, Science, Sports and Culture, Grant-in-Aid for Scientific Research (B), 15360100, 2005.

References

Bell, J.H., Mehta, R.D., 1990. Development of a two-stream mixing layer from tripped and untripped boundary layers. AIAA J. 28 (12), 2034–2042.

Kobashi, Y., 1957. Measurement of pressure fluctuation in the wake of cylinder. J. Phys. Soc. Jpn. 12 (5), 533–543.

Lueptow, R.M., Breuer, K.S., Haritonidis, J.H., 1988. Computer-aided calibration of X-probes using a look-up table. Exp. Fluids 6, 115–118.

Lumley, J.L., 1978. Computational modeling of turbulent flows. Adv. Appl. Mech. 18, 123–176.

Omori, T., Obi, S., Masuda, S., 2003. Experimental study on velocity–pressure correlation in turbulent mixing layer. In: Hanjalić, K. et al. (Eds.), Proc. Int. Symp. on Turbulence, Heat and Mass transfer, vol. 4, pp. 253–260.

Pope, S.B., 2000. Turbulent Flows. Cambridge University Press.

Rogers, M.M., Moser, R.D., 1994. Direct simulation of a self similar turbulent mixing layer. Phys. Fluids 6 (2), 903–922.

Shirahama, Y., Toyoda, K., 1993. Development of the probe to measure static-pressure fluctuations. Trans. JSME, Series B 59 (567), 3381–3387 (in Japanese).

Tsuji, Y., Ishihama, T., 2003. Similarity scaling of pressure fluctuation in turbulence. Phys. Rev. E 68, 026309.

Tsuji, Y., Fransson, J.H.M., Alfredsson, P.H., Johansson, A.V., 2005. Pressure statistics in high-Reynolds number turbulent boundary layer. In: Humphrey, J.A.C. et al. (Eds.), Proc. 4th Int. Symp. on Turbulence and Shear Flow Phenomena (TSFP-4), pp. 27–32.

Yao, Y.F., Thomas, T.G., Sandham, N.D., Williams, J.J.R., 2001. Direct numerical simulation of turbulent flow over a rectangular trailing edge. Theo. Comp. Fluid Dynam. 14, 337–358.